CHEMISTRY
A EUROPEAN JOURNAL

DOI: 10.1002/chem.201000839

# Rational Design of Nanofibers and Nanorings through Complementary Hydrogen-Bonding Interactions of Functional π Systems

Shiki Yagai,*[a, b] Hiroaki Aonuma,[a] Yoshihiro Kikkawa,[c] Shun Kubota,[a] Takashi Karatsu,[a] Akihide Kitamura,[a] Sankarapillai Mahesh,[d] and Ayyappanpillai Ajayaghosh*[d]

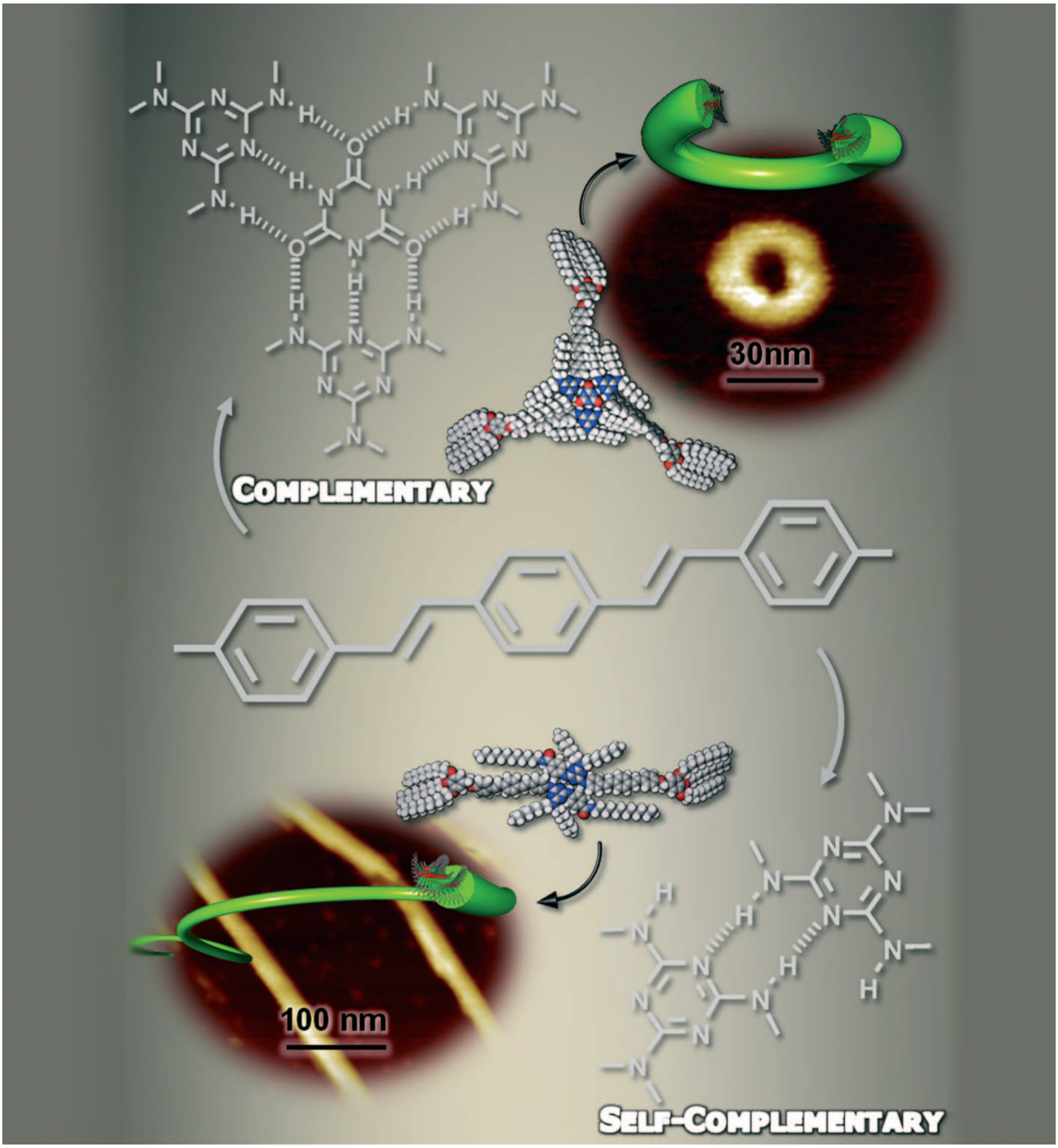

**Abstract:** A simple protocol to create nanofibers and -rings through a rational self-assembly approach is described. Whereas the melamine–oligo(*p*-phenylenevinylene) conjugate **1a** self-aggregates to form ill-defined nanostructures, conjugate **1b**, which possesses an amide group as an additional interactive site, self-aggregates to form 1D nanofibers that induce gelation of the solvent. AFM and XRD studies have shown that dimerization through the melamine–melamine hydrogen-bonding interaction occurs only for **1b**. Upon complexation with 1/3 equivalents of cyanuric acid (CA), conjugate **1a** provides well-defined, ring-shaped nanostructures at micromolar concentrations, which open to form fibrous assemblies at submillimolar concentrations and organogels in the millimolar concentration range. Apparently, the enhanced aggregation ability of **1a** by CA is a consequence of columnar organization of the resulting discotic complex $\mathbf{1a}_3$·CA. In contrast, coaggregation of **1b** with CA does not provide well-defined nanostructures, probably due to the interference of complementary hydrogen-bonding interactions by the amide group.

**Keywords:** gels · hydrogen bonds · nanostructures · oligomers · self-assembly

## Introduction

The construction of well-defined nanostructures from π-conjugated molecules is a subject of increasing research interest and underpins supramolecular electronics and photonics.[1] Whereas π-conjugated molecules have the intrinsic ability to self-assemble into extended 1D structures through π–π stacking interactions,[2] more precise control of their dimensionalities might be possible by using directional noncovalent interactions.[3] In this context, multiple hydrogen-bonding interactions between heterocyclic compounds are particularly appealing because of their selectivity and directionality,[4] offering shape-persistent supramolecular π-conjugated species that are capable of hierarchically assembling into well-defined functional nanostructures through π–π stacking interactions.[5] The elegance of this approach has been exemplified by the self-assembly of oligo(*p*-phenylenevinylene) (OPV) derivatives equipped with ureidotriazine[6] or melamine moieties.[7] The former OPV derivatives dimerize through quadruple hydrogen-bonding interactions, and subsequently organize to form twisted helical nanofibers. The latter OPV derivatives were found to form cylindrical nanotubes due to the formation of a cyclic hexamer (rosette) through double hydrogen bonding between melamine units. Thus, proper selection of a hydrogen-bonding motif enables the construction of different types of π-conjugated nanostructures.

We have been exploring two-component functional supramolecular assemblies based on multiple hydrogen-bonding interactions[8] due to their capability to produce diverse supramolecular species by minor structural modifications of either one of the two components,[9] or by changing their mixing ratio.[10] Self-assembly and photochemical properties of merocyanines and perylene bisimides have been successfully controlled through complementary triple hydrogen-bonding interactions between melamine donor–acceptor–donor (DAD) and imide acceptor–donor–acceptor (ADA) hydrogen-bonding units. We have recently shown that the self-assembly of the OPV **1a**, capped on one end by a monotopic melamine hydrogen-bonding module and the other end by a tridodecyloxyphenyl wedge,[11] can be controlled by complexation with cyanuric acid (CA) or substituted CA derivatives (ddCA or dCA) possessing differing numbers of ADA hydrogen-bonding sites (Scheme 1).[12] A particularly salient result was observed for the 3:1 mixture of **1a** with CA; this mixture provided organogels at millimolar concentrations as a consequence of columnar organization of the resulting complex. The self-aggregation of **1a** was also evidenced from the UV/Vis spectral study, but no morphological study has yet been addressed. Herein, we report a rational approach to control the self-aggregation of the melamine-capped OPV **1a** and its coaggregation with CA. To enhance the aggregation abilities of **1a** and its complex with CA, we have synthesized **1b**, which possesses an amide group as an additional hydrogen-bonding site.[13] In the present study, we underline that the presence of the amide group in **1b** dramatically affects the self- and coaggregation behavior leading to the controlled formation of rings and fibers.

[a] Prof. Dr. S. Yagai, H. Aonuma, S. Kubota, Prof. Dr. T. Karatsu, Prof. Dr. A. Kitamura
Department of Applied Chemistry and Biotechnology
Faculty of Engineering, Chiba University, 1-33 Yayoi-cho
Inage-ku, Chiba 263-8522 (Japan)
Fax: (+81) 43-290-3039
E-mail: yagai@faculty.chiba-u.jp

[b] Prof. Dr. S. Yagai
PRESTO (Japan) Science and Technology Agency (JST)
4-1-8 Honcho Kawaguchi, Saitama (Japan)

[c] Dr. Y. Kikkawa
Photonics Research Institute
National Institute of Advanced Industrial Science and Technology (AIST), 1-1-1 Higashi, Tsukuba, Ibaraki 305-8562 (Japan)

[d] S. Mahesh, Dr. A. Ajayaghosh
Photosciences and Photonics Group
Chemical Science and Technology Division
National Institute for Interdisciplinary Science and Technology (NIIST), CSIR, Trivandrum-695019 (India)
Fax: :(+91) 471-249-0186
E-mail: ajayaghosh62@gmail.com

Supporting information for this article is available on the WWW under http://dx.doi.org/10.1002/chem.201000839.

  

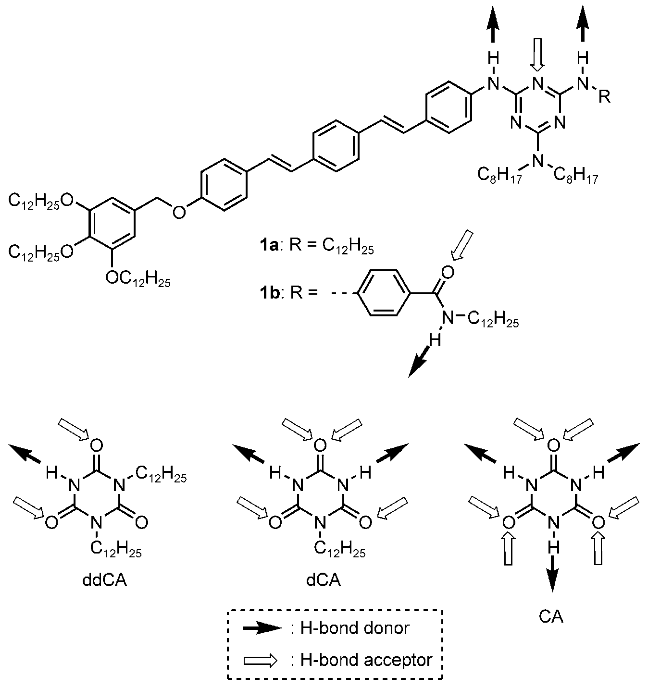


Scheme 1. Chemical structures of the melamine–oligo(*p*-phenylenevinylene) conjugates **1** and the complementary cyanurates.

## Results and Discussion

**Synthesis**: Compound **1b** was synthesized by the stepwise introduction of the aniline derivative **3** and dioctylamine onto the previously reported OPV **4** (Scheme 2).[14] Because of the relatively low reactivity of **3**, the synthesis of **1b** was carried out at 100 °C. After purification by column chromatography, compound **1b** was obtained in 45 % yield. The chemical structure of **1b** was confirmed by $^1$H NMR spectroscopy and MALDI-TOF and atmospheric pressure chemical ionization (APCI) mass spectrometry.

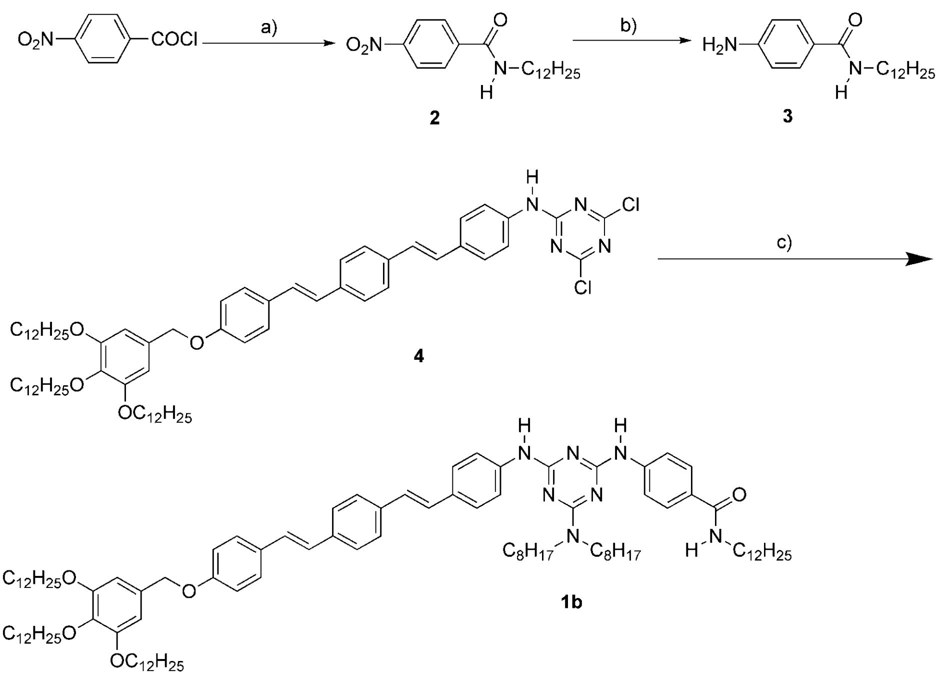


Scheme 2. Synthesis of **1b**: a) dodecylamine, pyridine, toluene, 80 °C, 3 h; b) hydrazine monohydrate, Pd/C, ethanol, 80 °C, 1 h; c) **3**, diisopropylethylamine, 1,4-dioxane, 100 °C, 12 h and then dioctylamine, reflux, 24 h.

**Optical properties**: The UV/Vis and fluorescence spectra of dilute solutions of **1a** and **1b** ($c = 1\times10^{-5}$ M) in chloroform and methylcyclohexane (MCH) were measured to compare their self-aggregating behavior. Both **1a** and **1b**, when dissolved in chloroform, show similar absorption and fluorescence bands arising from the π–π* transition of the molecularly dissolved OPV chromophores (Figures S1 and S2 in the Supporting Information).[14] This indicates that the phenylamido substituent of **1b** does not affect the intrinsic optical properties of OPV chromophores.

The OPV **1a** in MCH showed the π–π* transition at $\lambda_{max} = 376$ nm, which is identical to that observed in chloroform ($\lambda_{max} = 377$ nm), indicating that **1a** exists in the molecularly dissolved state (or more precisely, free from π–π stacking interactions) at this concentration (Figure S1 in the Supporting Information). The fluorescence spectrum of the solution in MCH is structured ($\lambda_{em\,max} = 415$ and 439 nm) when compared with that of the solution in chloroform (Figure S2 in the Supporting Information), however, no noticeable change is found for the peak positions, which again illustrates the absence of aggregation. Self-aggregation of **1a** starts to occur at around $c = 5\times10^{-4}$ M, shifting the π–π* transition to $\lambda_{max} = 365$ nm.[12] The fluorescence spectrum at this concentration (see Figure 2a, 0 equiv) does, however, show only a slight increase in the relative fluorescence intensity of the peak at 439 nm compared with that of the $1\times10^{-5}$ M solution (Figure 1). This observation indicates that the 365 nm absorbing species are weakly interacting molecular assemblies, which undergo rapid exchange with molecularly dissolved species.

Interestingly, the π–π* transition of the amide-functionalized **1b** in MCH at $c = 1\times10^{-5}$ M displayed a large shift towards $\lambda_{max} = 350$ nm with an appreciable hypochromic effect compared with that of **1a** (Figure 1). In the fluorescence spectrum, a significant decrease in the peak intensities at $\lambda =$ 415 and 439 nm are observed when compared with that of **1a**, whereas peaks in the longer wavelength region (at $\lambda = 469$, 500, and 540 nm) had increases in their intensities. These spectral changes are characteristic

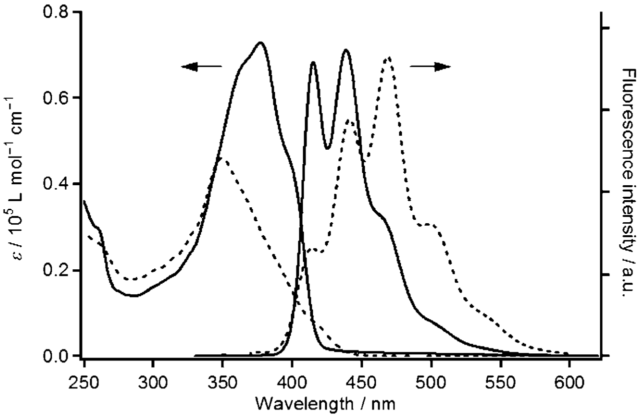


Figure 1. The UV/Vis (left axis) and fluorescence (right axis; $\lambda_{ex}$ = 349 nm) spectra of **1a** (solid line) and **1b** (dashed line) in MCH at 20 °C. Concentration: $1\times10^{-5}$ M.

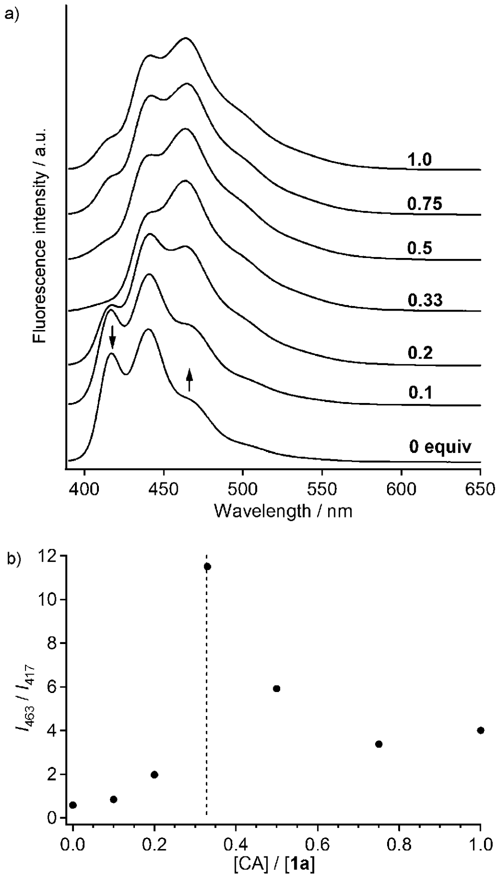


Figure 2. a) Fluorescence titration of **1a** ([**1a**] = $5\times10^{-4}$ M) with CA (0 to 1 equiv) in MCH; $\lambda_{ex}$ = 349 nm. The spectra were normalized at their maxima. Arrows indicate the changes upon an increase in the concentration of CA. b) Plot of the ratio of fluorescence intensities at $\lambda$ = 463 and 417 nm versus the [CA]/[**1a**] ratio. Dotted line indicates [CA]/[**1a**] = 0.33.

of the π–π stacking of OPV chromophores[6a,14,15] and demonstrate that the amide moiety of **1b** enhances the self-aggregation propensity of the melamine-capped OPV building blocks.

CA is a tritopic ADA-type hydrogen-bonding module that enables the trimerization of the melamine-capped OPVs through complementary hydrogen bonding.[16] The resulting 3:1 complex of **1** with CA has an expanded π surface, shifting the aggregation equilibrium towards a π–π stacked state, compared with **1** alone. We thus investigated the complexation of **1** with CA by using fluorescence spectroscopy because of its susceptibility to π–π stacking interactions. Figure 2a shows the fluorescence spectral change of **1a** with an increasing concentration of CA. The concentration of **1a** was set to $5\times10^{-4}$ M to ensure the presence of sufficient hydrogen-bonding interactions. Upon increasing the concentration of CA, the fluorescence peak at $\lambda$ = 417 nm derived from molecularly dissolved OPV chromophores decreased, and concurrently a new peak at $\lambda$ = 463 nm emerged as a result of π–π stacking of the OPV chromophores. When the ratio of these fluorescence peak intensities ($I_{463}/I_{417}$) was plotted against the molar ratio [CA]/[**1a**] the maximum was observed at [CA]/[**1a**] = 0.33 (Figure 2b), suggesting a 3:1 complexation between **1a** and CA. The quantitative binding of **1a** to all the ADA binding sites of CA under the present condition should, however, not be allowed if DAD–ADA hydrogen bonding is the only intermolecular interaction.[8c,17] Thus, it is believed that the resulting complexes were further stabilized by π–π stacking interactions as shown by the appreciable fluorescence spectral changes.

Of further interest is the reappearance of the fluorescence peak of the monomeric species at $\lambda$ = 417 nm upon the addition of greater amounts of CA ([CA]/[**1a**] > 0.33, Figure 2). This finding suggests that the mixing of the two components with the exact 3:1 molar ratio is a prerequisite for the formation of the complex **1a**$_3$·CA. In the presence of greater amounts of CA, additional hydrogen-bonded complexes, such as **1a**$_2$·CA and **1a**·CA, which have less tendency for aggregation through π–π stacking interactions, might be formed. These may even behave as terminating species in the hierarchical organization of **1a**$_3$·CA as inferred from the abrupt increase of the $I_{463}/I_{417}$ value at [CA]/[**1a**] = 0.33.

For the complex **1a**$_3$·CA, the formation of the two stereoisomers *i* and *ii*, shown in Figure 3a, should be considered with respect to the binding orientation of the three **1a** molecules. The stereoisomer *i* has a $C_3$-symmetrical structure, whereas *ii* is characterized by the presence of a π–π stacked OPV dimer within the structure. Such a dimeric unit can be produced by the 2:1 complexation of **1a** with the ditopic dCA (stereoisomer *iv* of **1a**$_2$·dCA in Figure 3b). To obtain information on the supramolecular structure of complex **1a**$_3$·CA, we compared the UV/Vis and fluorescence spectra of this complex with those of **1a**$_2$·dCA (Figure 3c and d). It has been revealed in a previous study that the 2:1 mixtures of **1a** and dCA in MCH show relatively sharp absorption spectra with blue-shifted maxima at around $\lambda$ = 355 nm over a wide concentration range ([**1a**] = $1\times10^{-6}$ to $5\times10^{-4}$ M, see Figure 3c for the spectrum of the $1\times10^{-5}$ M solution).[12] The large blue shift ($\lambda$ = 376→355 nm) and the concentration independence is consistent with the formation of the stereoisomer *iv* in which a π-stacked OPV dimer is locked by dCA through triple hydrogen-bonding interactions. In sharp

  

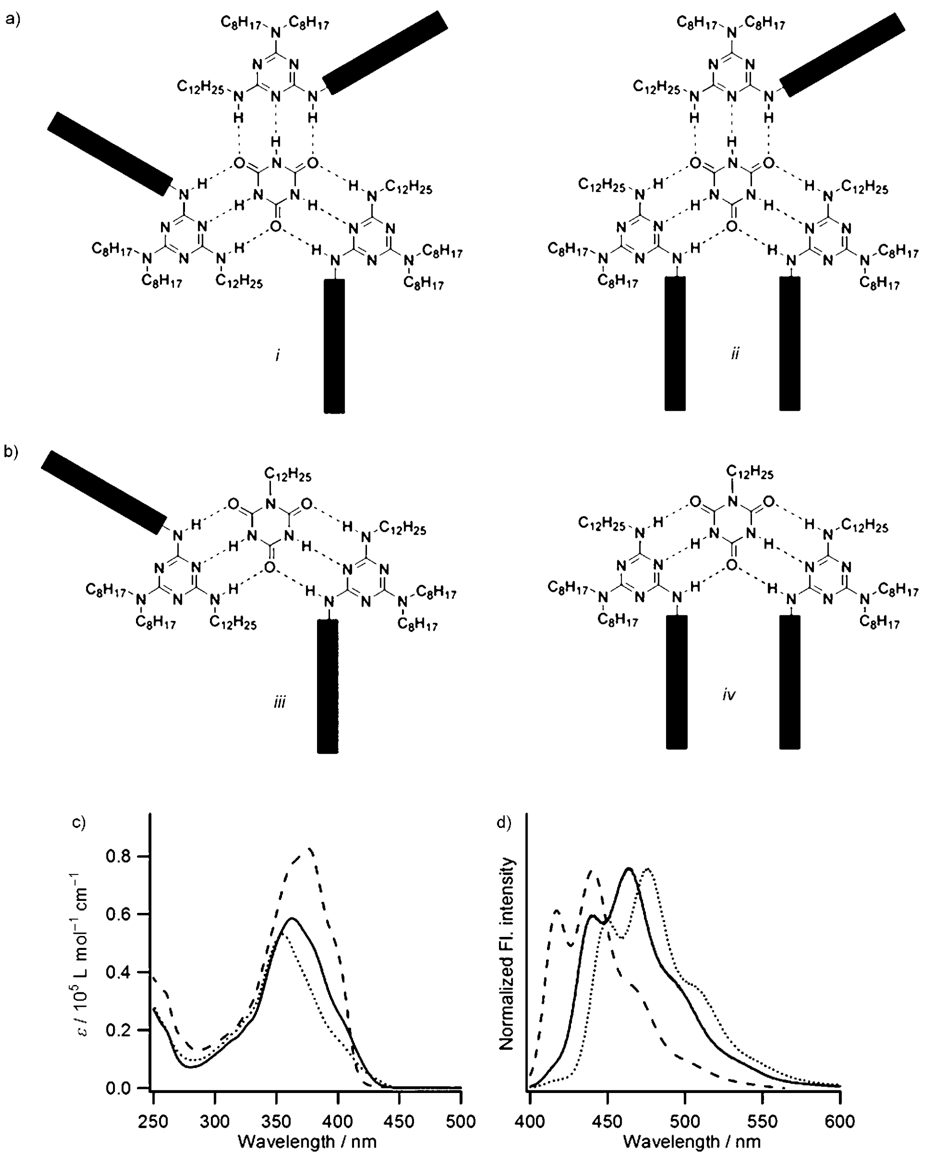


Figure 3. The possible stereoisomers of complexes a) $\mathbf{1a}_3$·CA and b) $\mathbf{1a}_2$·dCA. c) UV/Vis and d) fluorescence spectra of **1a** (dashed line, [**1a**]$=1\times10^{-5}$ M), $\mathbf{1a}_2$·dCA (dotted line, [**1a**]$=1\times10^{-5}$ M), and $\mathbf{1a}_3$·CA (solid line, [**1a**]$=5\times10^{-4}$ M) in MCH; $\lambda_{ex}=349$ nm. Different concentrations were chosen for the respective samples (see the text).

contrast, the absorption maxima of the 3:1 mixtures of **1a** and CA remain at $\lambda=376$ nm up to $1\times10^{-4}$ M, and shift to $\lambda=363$ nm at [**1a**]$=5\times10^{-4}$ M. A further increase in the concentration no longer impacts the absorption maximum. These observations clearly demonstrate that complex $\mathbf{1a}_3$·CA does not feature a π-stacked OPV dimer locked by CA. Moreover, the complex $\mathbf{1a}_2$·dCA emanates in a more red-shifted region than complex $\mathbf{1a}_3$·CA (Figure 3 d; $\lambda_{em\,max}=476$ nm for $\mathbf{1a}_2$·dCA and 463 nm for $\mathbf{1a}_3$·CA). The larger Stokes shift of $\mathbf{1a}_2$·dCA (121 nm) than that of $\mathbf{1a}_3$·CA (100 nm) can be rationalized by the formation of the stereoisomer *iv* in which the two OPV chromophores are strongly stacked within the complex (Figure 4 a). A closer inspection of the fluorescence spectrum of the complex $\mathbf{1a}_3$·CA revealed that there was no contamination of the fluorescence from such tightly interacting dimeric OPVs. Thus, it was concluded that complex $\mathbf{1a}_3$·CA does not form the stereoisomeric *ii*, and the observed spectral features of this complex emerging in [**1a**]$>5\times10^{-4}$ M are purely attributed to a hierarchical stacking of stereoisomer *i*. Why the complex $\mathbf{1a}_3$·CA does not take the stereoisomeric form *ii* is most likely to be due to the effective hierarchical organization of the $C_3$-symmetrical discotic structure of the stereoisomer *i* (Figure 4 b).

The complexation of **1b** with CA was also investigated with fluorescence spectroscopy, however, no notable spectral changes were observed. Two possibilities might be suggested for this result: 1) CA does not bind to **1b** due to the strong self-aggregation of **1b**; 2) CA binds to **1b** to form some kind of coaggregates in which the OPV chromophores are fully π–π stacked as in self-aggregated **1b**. This point is investigated by using AFM (see below).

**AFM analysis of nanostructures**: Solutions of **1a** ($c=5\times10^{-4}$ M) and **1b** ($c=1\times10^{-4}$ M) in MCH were spin-coated onto highly oriented pyrolytic graphite (HOPG) and the resulting nanostructures were visualized by AFM. The OPV **1a**, for which the UV/Vis data at this concentration showed the presence of π–π stacking, exhibited ill-defined nanostructures (Figure S3 in the Supporting Information). This observation indicates that **1a** has a low propensity to assemble well-de-

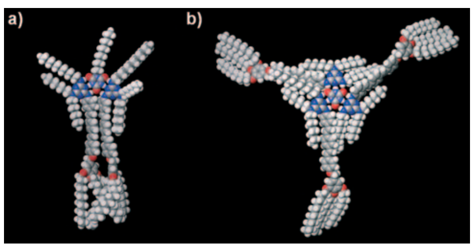


Figure 4. The energy-minimized structures of a) $\mathbf{1a}_2$·dCA (stereoisomeric form *iv*) and b) $\mathbf{1a}_3$·CA (stereoisomeric form *i*) obtained by molecular mechanical calculations.

  

fined nanostructures and hence nondirectional association occurs. On the contrary, well-defined fibrillar morphologies were visualized for **1b** (Figure 5a and b). The height of the elementary rod-shaped nanostructure is 8 nm (Figure 5c, d), twice the molecular length of **1b** with extended alkyl chains (see Figure 9f below). Thus, it is likely that **1b** forms dimers by hydrogen-bonding interactions between melamine moieties[7a,18] and the resulting dimers stack to form nanofibers that are stabilized by hydrogen bonding between amide groups (Scheme 3a). FTIR spectroscopy of thin films of **1b** exhibited an amide I band at 1631 $cm^{-1}$, confirming the formation of the hydrogen-bonding interaction. The dimerization of **1b** is further confirmed by the XRD study of the bulk material (see below).

Solutions of the melamine-capped OPVs ($c = 2\times10^{-4}$ M) in MCH containing 1/3 equivalents of CA were also spin-coated onto HOPG and imaged by AFM. Remarkably, the samples prepared from the mixtures of **1a** and CA showed agglomerated and isolated ring-shaped nanostructures (Figure 6a). Similar ring-shaped nanostructures have recently been discovered for small amphiphilic molecular building blocks[19] and several hydrogen-bonded disc-shaped assemblies (rosettes) by our group.[20] High-resolution AFM imaging of the nanorings revealed the size range of 20–50 nm with an average height of 3–4 nm. In sharp contrast to **1a**, CA had a negative effect on the self-assembly of the amide-functionalized **1b**. AFM images of the 3:1 mixture of **1b** and CA exhibited only amorphous structures. The fibrous nanostructures of **1b** completely disappeared upon the addition of CA (Figure S4 in the Supporting Information). This observation indicates that **1b** binds with CA, but the resulting coaggregates lack the ability to organize into well-de-

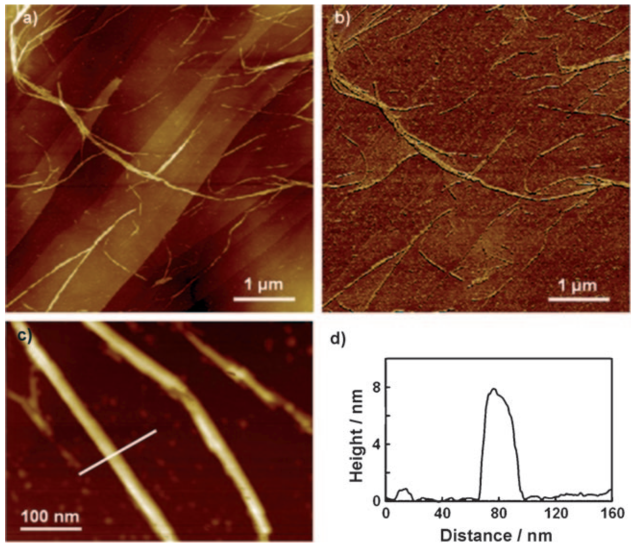


Figure 5. AFM a) height and b) phase images of self-aggregated **1b** spin-cast from a solution in MCH ($c = 1.0\times10^{-4}$ M) onto HOPG. c) Magnified AFM height image of elementary nanofibers of **1b** and d) cross-sectional analysis along the white line in c). $z$ scale = 30 nm in a) and 12 nm in c).

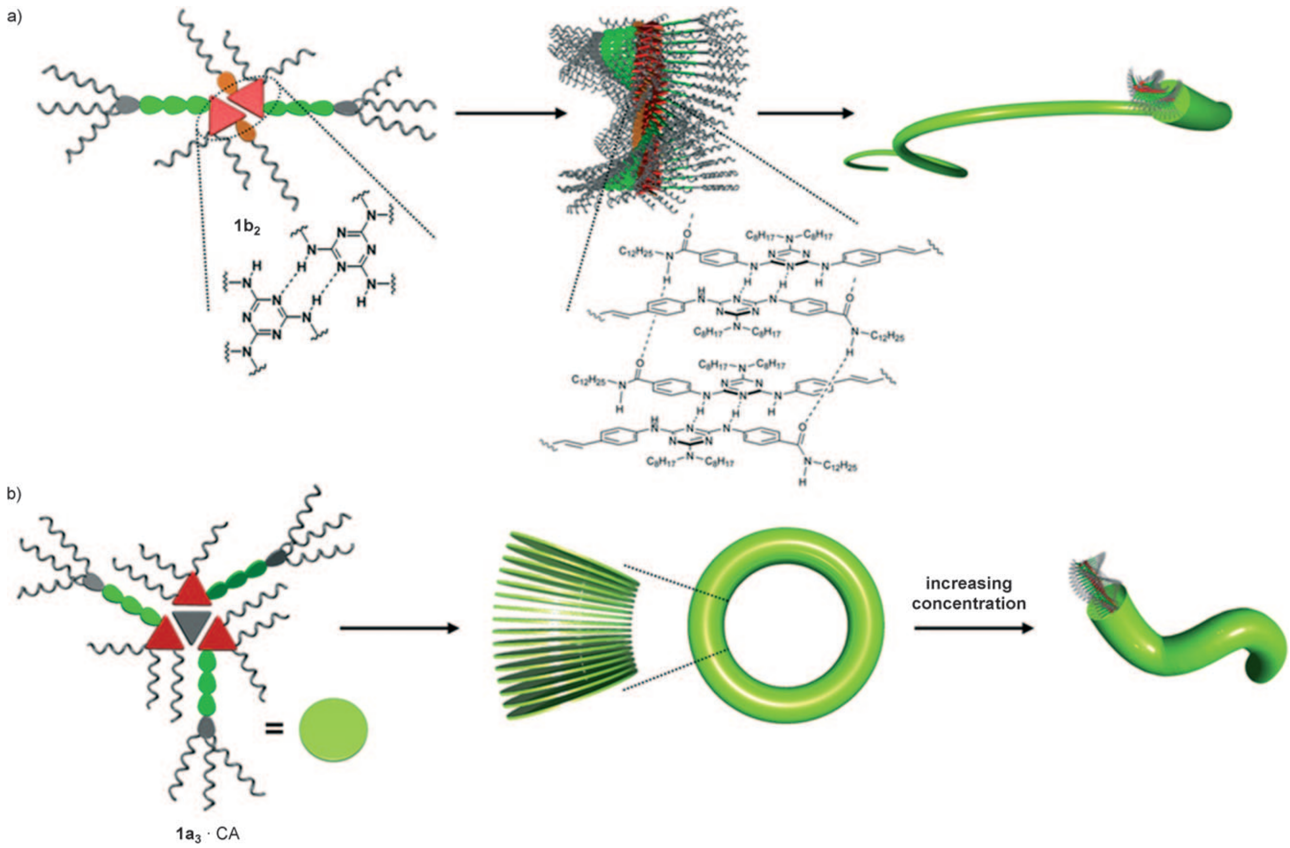


Scheme 3. Schematic representation of the a) self-aggregation of **1b** and b) coaggregation of **1a** with cyanuric acid (CA).

  

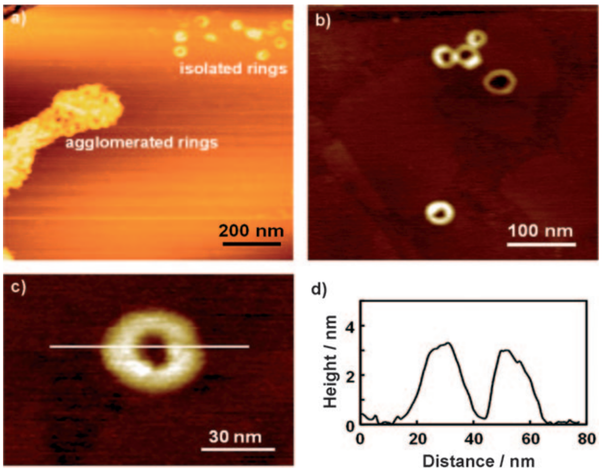


Figure 6. a–c) AFM height image of $1a_3$·CA spin-coated from a solution in MCH ($c=2.0\times10^{-4}$ M) and d) cross-sectional analysis along the white line in c). $z$ scale = 6 nm in a) and 5 nm in b).

fined nanostructures. Nonspecific hydrogen bonding between CA and the amide group of **1b** might occur to form various hydrogen-bonded coaggregates.

**Gelation**: Gelation of solvents by self-assembled, low-molecular-weight compounds is a good indicator of the formation of elongated fibrous nanostructures.[21] Furthermore, the formation of an organogel as a result of supramolecular organization of a small functional molecule, such as an OPV, allows the formation of optically and electronically active soft materials.[1,22] Appropriate amounts of **1a**, **1b**, and their 3:1 mixtures with CA were dissolved in MCH with heating, and the resulting homogeneous solutions were cooled to room temperature to examine the gelation behavior. Amide-functionalized **1b** instantly formed transparent gels with a concentration above $2\times10^{-3}$ M. This observation is in good agreement with the formation of 1D nanostructures visualized by AFM (Figure 5). In contrast, neither gels nor viscous liquids were formed for **1a** when homogeneous solutions ($\approx5\times10^{-3}$ M) were kept for several days. This observation is also consistent with the formation of ill-defined nanostructures revealed by AFM (Figure S3 in the Supporting Information).

Remarkably, the gelation abilities of **1a** and **1b** are reversed in the presence of 1/3 equivalents of CA. When a homogeneous solution of the 3:1 mixture of **1a** ($c=5\times10^{-3}$ M) and CA in MCH was kept at room temperature, a transparent gel was formed after one day. The AFM observation of a dried gel did not show any fibrous structures typically observed for low-molecular-weight gels (Figure 7a). Subsequently, the gel was diluted to $c=5\times10^{-4}$ M. The AFM images of the spin-cast solution exhibited short wormlike structures (Figure 7b), which are considered to be intermediate species between the gel-forming extended columnar structures and the nanorings formed in solutions at lower concentration (Scheme 3b). These structures were <300 nm in length and 10–30 nm in width.

**DLS analysis of nanostructures**: To support the formation of the nanostructures in solution, solutions of self- and coaggregates in MCH were assessed by dynamic light scattering (DLS). No analyzable particle was detected for the solutions of **1a** and $1b_3$·CA in the concentration ranging from $1\times10^{-4}$ to $5\times10^{-4}$ M, which is consistent with the results of the AFM studies. For a $1\times10^{-4}$ M solution of the amide-functionalized **1b**, however, extended assemblies with hydrodynamic diameters ($D_H$) close to 1 µm were detected (top data in Figure 8a). Interestingly, the average $D_H$ of the assemblies

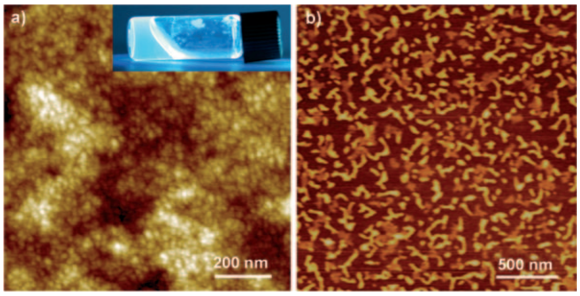


Figure 7. a) AFM height image of methylcyclohexane gel of $1a_3$·CA. $z$ scale = 10 nm. Inset shows a picture of the gel. b) AFM height image of $1a_3$·CA spin-cast from a solution in MCH ($c=5.0\times10^{-4}$ M). $z$ scale = 6 nm.

showed a time-dependent increase that exceeded 2 µm after 50 min (from top to bottom in Figure 8a). This is an indication of the presence of nonequilibrated extended supramolecular assemblies.

In contrast, solutions of $1a_3$·CA exhibited equilibrated, time-independent DLS results. For a $1\times10^{-4}$ M solution, assemblies for which the $D_H$ values were 60–90 nm were detected in addition to larger assemblies around 300–400 nm (Figure 8b). The former assemblies are believed to be the ring-shaped nanostructures observed by AFM. The smaller sizes of the rings observed by AFM compared with those from the DLS studies might be due to shrinkage of the sample during the evaporation of the solvent.[20a] The larger assemblies are, on the other hand, considered to be open-ended fibrous assemblies that are not detected by AFM. Upon increasing the concentration to $5\times10^{-4}$ M, the smaller assemblies clearly decreased, and the larger assemblies were the predominantly existing species (Figure 8c). These results agree well with the result of AFM studies and clearly demonstrate the concentration-dependent formation of closed and open structures of columnar stacks of the discotic supramolecular species $1a_3$·CA.[20b]

**Packing structures of OPV self-aggregates**: To gain a deeper insight into the dramatically different self-aggregation abilities of **1a** and **1b**, solid-state packing structures of these OPVs were investigated with polarized optical microscopy (POM), differential scanning calorimetry (DSC), and XRD techniques. The POM and DSC observations revealed that **1a** exhibits shearable birefringent mesophases between 71 (2.5 kJ mol$^{-1}$) and 85 °C (25.4 kJ mol$^{-1}$), and **1b** between 53

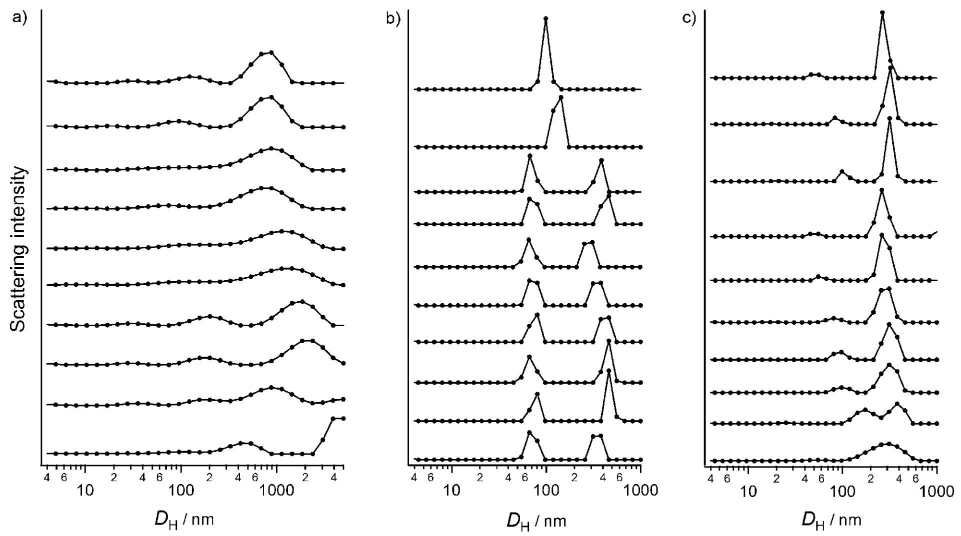


Figure 8. Time-dependent (from top to bottom) changes of the hydrodynamic diameter ($D_H$) distributions obtained by ten DLS measurements of solutions in MCH: a) **1b** ($1\times10^{-4}$ M), b) **1a**$_3$·CA ($1\times10^{-4}$ M), and c) **1a**$_3$·CA ($5\times10^{-4}$ M). Data acquisition was started 10 min after the preparation of sample solutions and were taken at 5 min intervals.

(1.1 kJ mol$^{-1}$) and 158 °C (10.3 kJ mol$^{-1}$). In the temperature ranges stated, the observed textures were easily broken by shearing. Above the temperature ranges, both compounds exist as isotropic liquids. The considerably different clearing temperatures suggest that the intermolecular interactions involved in the two mesophases are dramatically different. Upon cooling the isotropic liquids, shearable birefringent textures were observed for **1a** and **1b** (Figure 9a and b). These textures are considerably different from those of the columnar liquid crystalline mesophases of quadruply hydrogen-bonded OPV dimers.[23] The more well-defined fibrous texture of **1b** than that of **1a** is indicative of a higher degree of molecular ordering in the former mesophase.

The XRD pattern of **1a** in the mesophase showed broad reflections at 45.3, 22.6, and 17.8 Å (Figure 9c), demonstrating the formation of a lamellar structure with interlayer spacings around 45 Å. Since the molecular length of **1a** with a fully extended conformation is around 58 Å, a multilamellar packing of **1a** with interdigitation of alkyl chains is strongly suggested (Figure 9e).[24] This observation excludes the possibility of dimerization of **1a** by melamine–melamine hydrogen-bonding interactions. In contrast, compound **1b** showed much sharper XRD peaks at 73.6, 36.3, and 25.0 Å with several unidentifiable peaks, indicating the formation of a more ordered multilamellar structure (Figure 9d). Interestingly, the interlayer spacing of **1b** (73.6 Å) is much longer than that of **1a**. Significantly, different interlayer spacings between the two compounds cannot be explained by the difference in their molecular lengths (**1a** = 58 and **1b** = 65 Å). Combined with the formation of fibrous nanostructures with the width of 8 nm (Figure 5), it is strongly suggested that **1b** dimerizes by hydrogen-bonding interactions between the melamine moieties, and the resulting dimer is the building block for the extended self-assembled architectures (Figure 9f). The occurrence of dimerization in the self-aggregation of **1b** might be due to the stabilization of the resulting dimers by hierarchical organization through two-point hydrogen-bonding interactions between amide functionalities and π–π stacking interaction (Scheme 3a).

## Conclusion

By the exploitation of the existing knowledge of the self-assembly behavior of OPVs in conjunction with the multiple hydrogen-bonding melamine moiety, we could rationally design molecular systems that self- and coassemble into supramolecular architectures with distinct morphologies. Thus, we could demonstrate that the melamine-capped OPV **1a** self-aggregated to form ill-defined structures, and coaggregated with CA at low concentrations to form nanorings and at high concentrations to form open structures, leading to the gelation of solvents. On the other hand, the OPV **1b**, which has an additional amide group, self-assembled to form nanofibers, leading to gelation of solvents. The coassembly of CA with **1b** resulted in ill-defined structures with gelation abilities. By using spectroscopic, DLS, and AFM analyses, it was revealed that the amide group strongly enhances the self-aggregation of the melamine-capped OPV building blocks. XRD in the liquid-crystalline state suggested that dimerization by melamine–melamine hydrogen-bonding interactions occur only for the amide derivative, thereby enhancing its self-aggregation ability. The poor aggregation ability of the melamine-capped OPV lacking the amide group could be improved by the addition of 1/3 equivalents of CA due to the formation of $C_3$-symmetrical hydrogen-bonded discs. Such discs possessing three OPV π systems hierarchically organized in a nonpolar solvent to form a ring-shaped morphology at micromolar concentrations and gel-forming extended columnar structures at millimolar concentrations. Thus, the present study demonstrates the possibility of constructing defined supramolecular architectures with melamine-capped π-conjugated molecules. We are currently applying the present molecular design strategy to the creation of various π-conjugated functional architectures with defined size and shape.

## Acknowledgements

This work was partially supported by a Grant-in-Aid for Scientific Research from the Japan Society for the Promotion of Science (JSPS). S.Y., S.M., A.A., and A.K. thank the Department of Science and Technology,

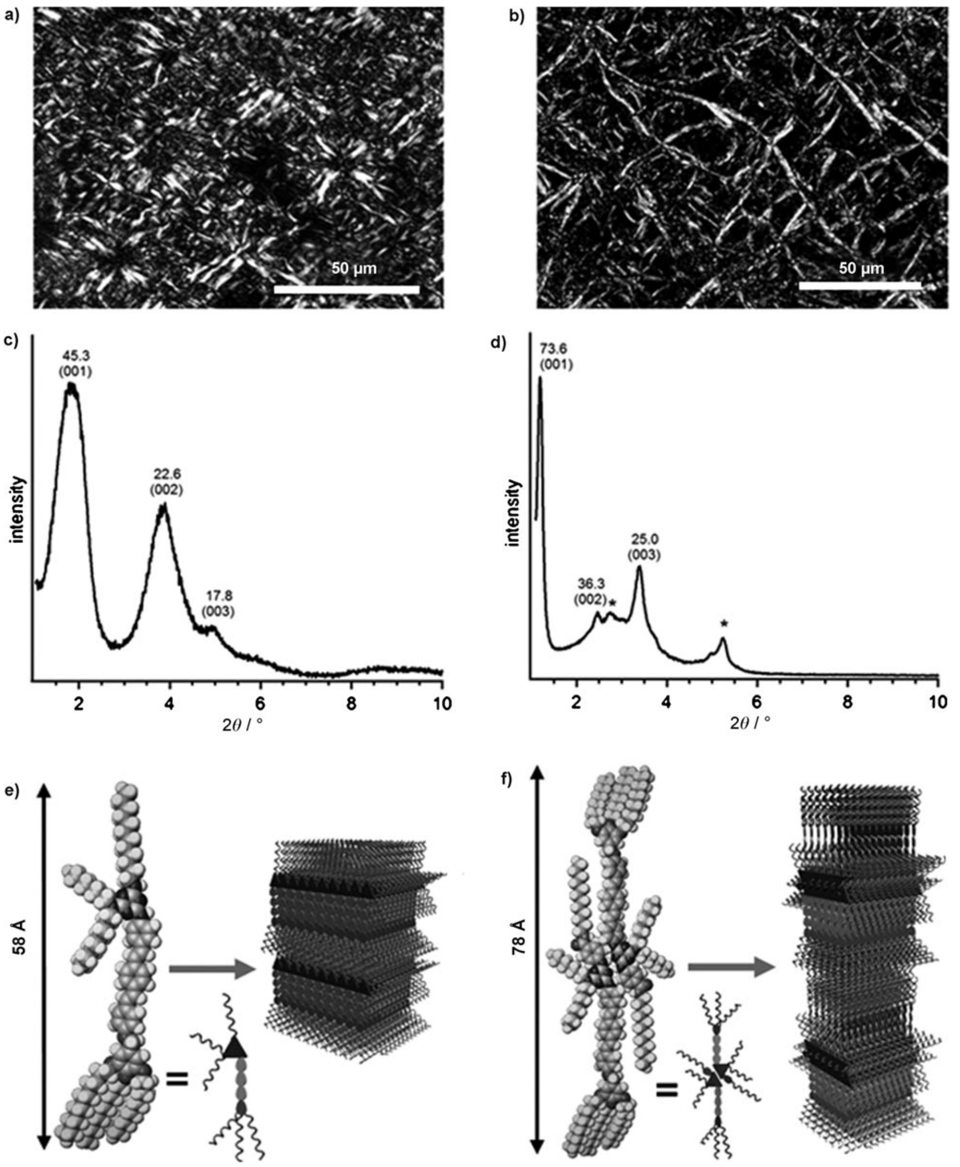


Figure 9. Polarized optical micrographs (a, b), XRD patterns (c, d), and proposed lamellar packing structures (e, f) of **1a** (a, c, e) at 75 °C and **1b** (b, d, f) at 175 °C upon cooling from the isotropic melt (cooling rate = 1 °C $min^{-1}$). The peaks designated by asterisk in d) are unidentified peaks.

New Delhi and the Japan Society for the Promotion of Science, Japan for financial support. S. Mahesh thanks the University Grants Commission, New Delhi for a fellowship. We thank Dr. Yasuo Norikane of the National Institute of Advanced Industrial Science and Technology (AIST), Tsukuba, for the measurement of MALDI-TOF MS spectrometry.

[1] a) F. Würthner, *Chem. Commun.* **2004**, 1564–1579; b) A. F. J. M. Hoeben, P. Jonkheijm, E. W. Meijer, A. P. H. J. Schenning, *Chem. Rev.* **2005**, *105*, 1491–1546; c) J. W. W. Pisula, K. Müllen, *Chem. Rev.* **2007**, *107*, 718–747; d) A. Ajayaghosh, V. K. Praveen, *Acc. Chem. Res.* **2007**, *40*, 644–656; e) L. Zang, Y. Che, J. S. Moore, *Acc. Chem. Res.* **2009**, *42*, 1596–1608; f) V. Percec, M. Glodde, T. K. Bera, Y. Miura, I. Shiyanovskaya, K. D. Singer, V. S. K. Balagurusamy, P. A. Heiney, I. Schnell, A. Rapp, H. W. Spiess, S. D. Hudson, H. Duan, *Nature* **2002**, *417*, 384–387; g) J. P. Hill, W. Jin, A. Kosaka, T. Fukushima, H. Ichihara, T. Shimomura, K. Ito, T. Hashizume, N. Ishii, T. Aida, *Science* **2004**, *304*, 1481–1483.

[2] C. A. Hunter, J. K. M. Sanders, *J. Am. Chem. Soc.* **1990**, *112*, 5525–5534.

[3] a) G. M. Whitesides, J. P. Mathias, C. T. Seto, *Science* **1991**, *254*, 1312–1319; b) J.-M. Lehn, *Supramolecular Chemistry: Concepts and Perspectives*, VCH, Weinheim, **1995**; c) T. Kato, *Struct. Bonding (Berlin)* **2000**, *96*, 95–146.

[4] a) G. M. Whitesides, E. E. Simanek, J. P. Mathias, C. T. Seto, D. Chin, M. Mammen, D. M. Gordon, *Acc. Chem. Res.* **1995**, *28*, 37–44; b) S. C. Zimmerman, P. S. Corbin, *Struct. Bonding (Berlin)* **2000**, *96*, 63–94; c) M. W. Peczuh, A. D. Hamilton, *Chem. Rev.* **2000**, *100*, 2479–2494; d) L. J. Prins, D. N. Reinhoudt, P. Timmerman, *Angew. Chem.* **2001**, *113*, 2446–2492; *Angew. Chem. Int. Ed.* **2001**, *40*, 2382–2426; e) R. P. Sijbesma, E. W. Meijer, *Chem. Commun.* **2003**, 5–16; f) S. Lena, S. Masiero, S. Pieraccini, G. P. Spada, *Chem. Eur. J.* **2009**, *15*, 7792–7806; g) U. Drechsler, B. Erdogan, V. M. Rotello, *Chem. Eur. J.* **2004**, *10*, 5570–5579; h) S. Yagai, *J. Photochem. Photobiol. C* **2006**, *7*, 164–182.

[5] a) H. M. Keizer, R. P. Sijbesma, *Chem. Soc. Rev.* **2005**, *34*, 226–234; b) T. Kato, T. Yasuda, Y. Kamikawa, M. Yoshio, *Chem. Commun.* **2009**, 729–739; c) T. Kato, N. Mizoshita, K. Kishimoto, *Angew. Chem.* **2006**, *118*, 44–74; *Angew. Chem. Int. Ed.* **2006**, *45*, 38–68.

[6] a) P. Jonkheijm, F. J. M. Hoeben, R. Kleppinger, J. Van Herrikhuyzen, A. P. H. J. Schenning, E. W. Meijer, *J. Am. Chem. Soc.* **2003**, *125*, 15941–15949; b) P. Jonkheijm, P. P. A. M. van der Schoot, A. P. H. J. Schenning, E. W. Meijer, *Science* **2006**, *313*, 80–83; c) S. J. George, Z. Tomovic, M. M. J. Smulders, T. F. A. d. Greef, P. E. L. G. Leclere, E. W. Meijer, A. P. H. J. Schenning, *Angew. Chem.* **2007**, *119*, 8354–8359; *Angew. Chem. Int. Ed.* **2007**, *46*, 8206–8211.

[7] P. Jonkheijm, A. Miura, M. Zdanowska, F. J. M. Hoeben, S. De Feyter, A. P. H. J. Schenning, F. C. De Schryver, E. W. Meijer, *Angew. Chem.* **2004**, *116*, 76–80; *Angew. Chem. Int. Ed.* **2004**, *43*, 74–78.

[8] For examples of two-component functional dye assemblies based on multiple hydrogen-bonding interactions, see: a) M. Kotera, J. M. Lehn, J. P. Vigneron, *J. Chem. Soc. Chem. Commun.* **1994**, 197–199; b) N. Kimizuka, T. Kawasaki, K. Hirata, T. Kunitake, *J. Am. Chem. Soc.* **1995**, *117*, 6360–6361; c) F. Würthner, C. Thalacker, A. Sautter, W. Schartl, W. Ibach, O. Hollricher, *Chem. Eur. J.* **2000**, *6*, 3871–3886; d) F. Würthner, S. Yao, B. Heise, C. Tschierske, *Chem. Commun.* **2001**, 2260–2261; e) L. J. Prins, C. Thalacker, F. Würthner, P. Timmerman, D. N. Reinhoudt, *Proc. Natl. Acad. Sci. USA* **2001**, *98*, 10042–10045; f) A. P. H. J. Schenning, V. H. Jeroen, P. Jonkheijm, Z. Chen, F. Würthner, E. W. Meijer, *J. Am. Chem. Soc.* **2002**,

  

*124*, 10252–10253; g) F. Würthner, S. Yao, *J. Org. Chem.* **2003**, *68*, 8943–8949; h) F. J. M. Hoeben, M. J. Pouderoijen, A. P. H. J. Schenning, E. W. Meijer, *Org. Biomol. Chem.* **2006**, *4*, 4460–4462; i) H. Nakade, B. J. Jordan, H. Xu, G. Han, S. Srivastava, R. R. Arvizo, G. Cooke, V. M. Rotello, *J. Am. Chem. Soc.* **2006**, *128*, 14924–14929; j) A. Llanes-Pallas, C.-A. Palma, L. Piot, A. Belbakra, A. Listorti, M. Prato, P. Samori, N. Armaroli, D. Bonifazi, *J. Am. Chem. Soc.* **2009**, *131*, 509–520; k) K. Yoosaf, A. Belbakra, N. Armaroli, A. Llanes-Pallas, D. Bonifazi, *Chem. Commun.* **2009**, 2830–2832.

[9] a) S. Yagai, M. Higashi, T. Karatsu, A. Kitamura, *Chem. Mater.* **2004**, *16*, 3582–3585; b) S. Yagai, M. Higashi, T. Karatsu, A. Kitamura, *Chem. Mater.* **2005**, *17*, 4392–4398; c) S. Yagai, M. Higashi, T. Karatsu, A. Kitamura, *Chem. Commun.* **2006**, 1500–1502; d) S. Yagai, T. Kinoshita, M. Higashi, K. Kishikawa, T. Nakanishi, T. Karatsu, A. Kitamura, *J. Am. Chem. Soc.* **2007**, *129*, 13277–13287; e) S. Yagai, Y. Monma, N. Kawauchi, T. Karatsu, A. Kitamura, *Org. Lett.* **2007**, *9*, 1137–1140; f) T. Seki, S. Yagai, T. Karatsu, A. Kitamura, *J. Org. Chem.* **2008**, *73*, 3328–3335; g) T. Seki, S. Yagai, T. Karatsu, A. Kitamura, *Chem. Lett.* **2008**, *37*, 764–765; h) S. Yagai, T. Kinoshita, Y. Kikkawa, T. Karatsu, A. Kitamura, Y. Honsho, S. Seki, *Chem. Eur. J.* **2009**, *15*, 9320–9324.

[10] a) S. Yagai, T. Seki, T. Karatsu, A. Kitamura, F. Würthner, *Angew. Chem.* **2008**, *120*, 3415–3419; *Angew. Chem. Int. Ed.* **2008**, *47*, 3367–3371; b) S. Yagai, S. Hamamura, H. Wang, V. Stepanenko, T. Seki, K. Unoike, Y. Kikkawa, T. Karatsu, A. Kitamura, F. Würthner, *Org. Biomol. Chem.* **2009**, *7*, 3926–3929; c) S. Mahesh, R. Thirumalai, S. Yagai, A. Kitamura, A. Ajayaghosh, *Chem. Commun.* **2009**, 5984–5986; d) T. Tazawa, S. Yagai, Y. Kikkawa, T. Karatsu, A. Kitamura, A. Ajayaghosh, *Chem. Commun.* **2010**, *46*, 1076–1078.

[11] B. M. Rosen, C. J. Wilson, D. A. Wilson, M. Peterca, M. R. Imam, V. Percec, *Chem. Rev.* **2009**, *109*, 6275–6540.

[12] S. Yagai, S. Kubota, K. Unoike, T. Karatsu, A. Kitamura, *Chem. Commun.* **2008**, 4466–4468.

[13] a) Y. Kobayashi, Y. Matsunaga, *Bull. Chem. Soc. Jpn.* **1987**, *60*, 3515–3518; b) A. J. Wilson, M. Masuda, R. P. Sijbesma, E. W. Meijer, *Angew. Chem.* **2005**, *117*, 2315–2319; *Angew. Chem. Int. Ed.* **2005**, *44*, 2275–2279; c) F. Würthner, C. Bauer, V. Stepanenko, S. Yagai, *Adv. Mater.* **2008**, *20*, 1695–1698.

[14] S. Yagai, S. Kubota, T. Iwashima, K. Kishikawa, T. Nakanishi, T. Karatsu, A. Kitamura, *Chem. Eur. J.* **2008**, *14*, 5246–5257.

[15] a) J.-F. Eckert, J.-F. Nicoud, J.-F. Nierengarten, S.-G. Liu, L. Echegoyen, F. Barigelletti, N. Armaroli, L. Ouali, V. Krasnikov, G. Hadziioannou, *J. Am. Chem. Soc.* **2000**, *122*, 7467–7479; b) S. J. George, A. Ajayaghosh, *Chem. Eur. J.* **2005**, *11*, 3217–3227; c) B. W. Messmore, J. F. Hulvat, E. D. Sone, S. I. Stupp, *J. Am. Chem. Soc.* **2004**, *126*, 14452–14458; d) J. F. Hulvat, M. Sofos, K. Tajima, S. I. Stupp, *J. Am. Chem. Soc.* **2005**, *127*, 366–372; e) K. Tajima, L.-S. Li, S. I. Stupp, *J. Am. Chem. Soc.* **2006**, *128*, 5488–5495.

[16] M. Arduini, M. Crego-Calama, P. Timmerman, D. N. Reinhoudt, *J. Org. Chem.* **2003**, *68*, 1097–1106.

[17] F. J. M. Hoeben, J. Zhang, C. C. Lee, M. J. Pouderoijen, M. Wolffs, F. Würthner, A. P. H. J. Schenning, E. W. Meijer, S. De Feyter, *Chem. Eur. J.* **2008**, *14*, 8579–8589.

[18] a) J. Barberá, L. Puig, J. L. Serrano, T. Sierra, *Chem. Mater.* **2004**, *16*, 3308–3317; b) J. Barberá, L. Puig, P. Romero, J. L. Serrano, T. Sierra, *J. Am. Chem. Soc.* **2005**, *127*, 458–464.

[19] J.-K. Kim, E. Lee, Z. Huang, M. Lee, *J. Am. Chem. Soc.* **2006**, *128*, 14022–14023.

[20] a) S. Yagai, S. Mahesh, Y. Kikkawa, K. Unoike, T. Karatsu, A. Kitamura, A. Ajayaghosh, *Angew. Chem.* **2008**, *120*, 4769–4772; *Angew. Chem. Int. Ed.* **2008**, *47*, 4691–4694; b) S. Yagai, S. Kubota, H. Saito, K. Unoike, T. Karatsua, A. Kitamura, A. Ajayaghosh, M. Kanesato, Y. Kikkawa, *J. Am. Chem. Soc.* **2009**, *131*, 5408–5410.

[21] a) P. Terech, R. G. Weiss, *Chem. Rev.* **1997**, *97*, 3133–3160; b) J. H. Van Esch, B. L. Feringa, *Angew. Chem.* **2000**, *112*, 2351–2354; *Angew. Chem. Int. Ed.* **2000**, *39*, 2263–2266; c) L. A. Estroff, A. D. Hamilton, *Chem. Rev.* **2004**, *104*, 1201–1218; d) N. M. Sangeetha, U. Maitra, *Chem. Soc. Rev.* **2005**, *34*, 821–836; e) T. Ishi-i, S. Shinkai, *Top. Curr. Chem.* **2005**, *258*, 119–160.

[22] a) A. Ajayaghosh, S. J. George, A. P. H. J. Schenning, *Top. Curr. Chem.* **2005**, *258*, 83–118; b) A. Ajayaghosh, C. Vijayakumar, V. K. Praveen, S. S. Babu, R. Varghese, *J. Am. Chem. Soc.* **2006**, *128*, 7174–7175; c) A. Ajayaghosh, V. K. Praveen, C. Vijayakumar, S. J. George, *Angew. Chem.* **2007**, *119*, 6376–6381; *Angew. Chem. Int. Ed.* **2007**, *46*, 6260–6265; d) A. Ajayaghosh, V. K. Praveen, S. Srinivasan, R. Varghese, *Adv. Mater.* **2007**, *19*, 411–415; e) A. Ajayaghosh, V. K. Praveen, C. Vijayakumar, *Chem. Soc. Rev.* **2008**, *37*, 109–122.

[23] W. Pisula, Z. Tomovic, M. Wegner, R. Graf, B. Maarten, J. Pouderoijen, E. W. Meijer, A. P. H. J. Schenning, *J. Mater. Chem.* **2008**, *18*, 2968–2977.

[24] The antiparallel packing of **1a** within a layer may be another proposed structure.

Received: April 3, 2010
Published online: July 7, 2010

  